Optimal Design of Grid Tied PV System Using Manta Rays Foraging Optimizer

Ahmed M. Abdelmohsen, Ahmed M. Hussien, and Omar M. Yasser
Electric Power and Machines Dept, Faculty of Engineering, Ain Shams University, Egypt

16E0024@eng.asu.edu.eg, 16E0018@eng.asu.edu.eg, 1600915@eng.asu.edu.eg,

Supervisor: Prof. Dr. Hany M. Hassanien, Prof. Dr. Gamal M. Hashem
Faculty of Engineering, Ain Shams University, Egypt, hanyhasanien@ieee.org , gamal_hashem@eng.asu.edu.eg

***Abstract*— In the past few years, the photovoltaic (PV) power generation has received a lot of attention due to its cost effectiveness and as one of the most proliferating renewable energy sources. Owing to PV stations spreading, the effect of these stations on the power system became a major concern. This paper investigates the control of large-scale PV systems under normal and faulty circumstances. The PV system comprised of a regulated boost DC-DC converter and a three-phase inverter. For grid integration, a filter and a step-up transformer were used. Incremental Conductance Maximum Power Point Tracking Algorithm is used to control the duty cycle of the boost converter. A synchronous d-q frame voltage and current cascaded loop control scheme that employed Proportional Integral (PI) controllers is used for controlling the power injected by the inverter. The optimal PI coefficients were acquired by employing the Metaheuristic Manta ray foraging optimization technique. For the purposes of simulating the proposed control strategy, MATLAB/Simulink-Simscape software is used. Furthermore, to validate the adequacy of the control strategy in riding through the faults, the PV system response is assessed under various faulty circumstances.**

I. INTRODUCTION

Industrialization and population growth have propelled the world energy demand on an upwards climb over the past years. This has influenced the demand for renewable energy sources such as photovoltaic (PV); making it more popular for sustainability with enormous potential. The role of power electronics and their associated control methodologies are critical for reliable and efficient operation of these PV systems.

PHOTOVOLTAIC (PV) system will be one of the most promising renewable energy systems in the near future. The costs of the installed PV systems are continuously decreasing worldwide because of falling component average selling prices. Based on the statistics of the PV power plants 2014 industry guide report, the global PV system installations reached 136.7 GW at the end of 2013 and the cumulative market growth reaches 36%. Several factors affect the high penetration of the PV systems into electricity networks, such as environmental concerns, clean energy, increase in fuel price, political issues, and PV system cost reduction. In addition, installations of the MW PV power plants take only a few months. Large scale PV power plants were connected to the electric grid in the last few years. Because of this large integration with the electric grid, many problems arise and need to solve like low voltage ride through (LVRT) capability enhancement of such systems. With the high level of penetration of the PV power plants in the electric grids, maintaining the grid stability and reliability represents a greater challenge to the network operators. Recently, the utilities have released medium voltage grid codes to the PV systems that impose on these systems to contribute to and have a role in the grid support during grid faults. To fulfill these grid codes, the PV system needs to satisfy the LVRT capability requirement and remains in the grid-connected mode immediately after a disturbance takes place. Several methods have been used to study, analyze, and improve the LVRT capability of the PV systems. In, the LVRT capability of single-phase grid-connected PV systems was presented using an extensive control method, which depends on controlling both the real and reactive powers out of the PV system.

Over the years researchers utilize various types of controllers such as the Proportional Integral (PI) and PI-Derivative (PID) to control PV inverters. In (2013) a researcher compared outputs from a PI based current regulator optimized by Particle Swarm (PSO), Genetic Algorithm (GA) and Ziegler-Nichol's optimization techniques to determine the optimal PI gains. A fixed switching frequency was employed and the PSO provided the best results. In 2018 the concept of controlling the active and reactive power of a PV inverter output using an H-bridge topology. DC-DC converter in conjunction with an inverter was presented. The inverter control was implemented using pulse width modulation (PWM) and an auto coupler pulse transformer. A PI compensator was used for DC voltage stabilization. Some works also considered the application of PI, Proportional Resonant Integral (PRI), Quasi-Proportional Resonance (QPR) control methods in single phase PV systems to mitigate harmonic distortion and improve system performance.
The paper is organized as follows:

(Section II describes the PV power plant model. In Section III, describes tuning PIDs using MRFO, and Section IV evaluates system performance under fault conditions

5th IUGRC International Undergraduate Research Conference,
Military Technical College, Cairo, Egypt, Aug 9th – Aug 12th, 2021.

II. Steady State Control

We Simulated a 100 kW PV system connected to utility grid by a 400v/25kv D-Y Transformer as shown in Fig.2

A. Maximum Power Point Tracker (MPPT)

the ICT MPPT is among the popular techniques for its simplicity and efficiency in MPP extraction; however, it suffers from a poor dynamic performance. This poor dynamic performance is highly attributed to the use of fixed step of the duty cycle for the DC-DC converter for tracking the MPP. If the fixed step in the duty cycle is large, the MPPT will accelerate the operating point toward the MPP; however, there will be sustained oscillations around the MPP as the need precise value of the duty cycle for operation at the MPP is not found. For enhancing the ICT algorithm which will be called the Integral Regulator & Incremental Conductance (I&IC) algorithm.

As an enhancement to the incremental conductance technique, an integral regulator was added to it to minimize the error and optimize the duty cycle correction factor. In incremental conductance technique the error equals to

$$error = \frac{dI}{dV} + \frac{I}{V} \qquad (1)$$

The error signal is the input to a PID Controller that

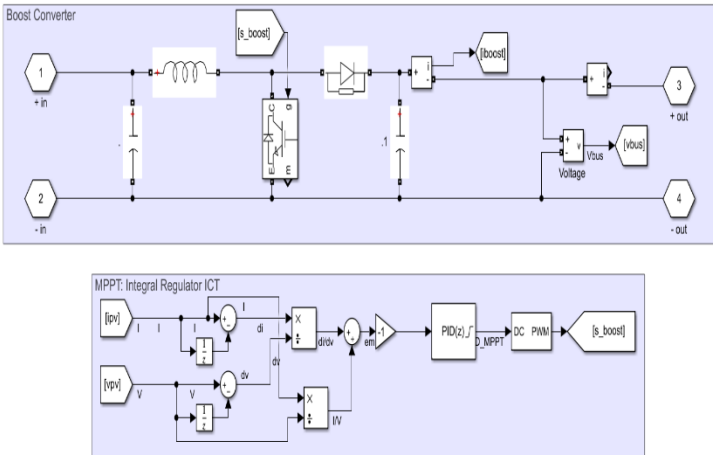

Fig. 1 MPPT circuit and control technique

determines the duty cycle of the boost converter as shown in Fig.1

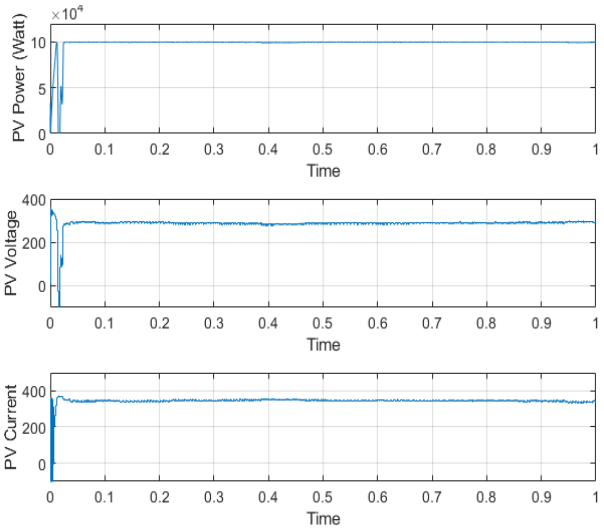

Simulation results of this stage are as following

Fig. 3 MPPT Simulation Results

B. Inverter Control (Current Loop Control):

In order to maintain system stability during transients and fault and protect inverter from both over current and voltage, we used a cascaded control scheme that generates reference current values in order to maintain both AC and DC voltages at the required levels. Those reference values will be limited by the inverter current rating. The reference signals are used in the inner loop to generate SPWM that maintains currents at the required levels.

This Control in done based on the following Equations:

In the dq0 reference frame, the active and reactive power values are given by the following equations,

$$P = \frac{3}{2}\left(V_d I_d + V_q I_q\right) \qquad (2)$$

$$Q = \frac{3}{2}\left(-V_d I_q + V_q I_d\right) \qquad (3)$$

V_q is set to zero by the PLL. Therefore, the decoupling between the active and reactive power is achieved as,

$$P = \frac{3}{2}\left(V_d I_d\right) \qquad (4)$$

$$Q = \frac{3}{2}\left(-V_d I_q\right) \qquad (5)$$

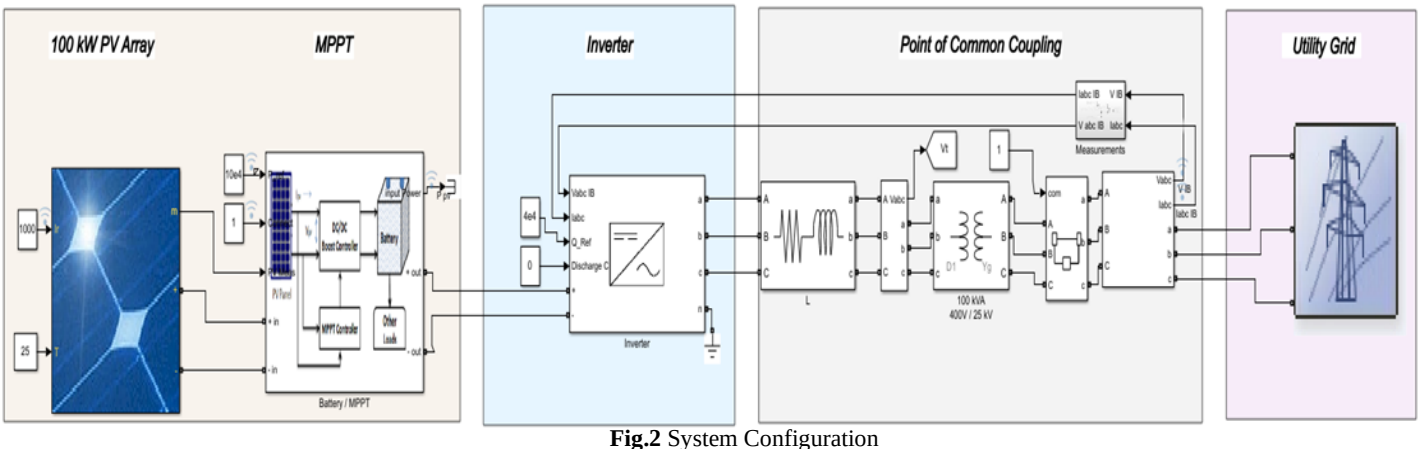

Fig.2 System Configuration

The active and reactive power can be then controlled by controlling I_d and I_q respectively. The reference direct-axis current (Id_ref) has been calculated as explained before. The quadrature axis current reference (Iq_ref) is determined according to the inverter mode of operation.

The function of current regulator block is to make the inverter output current rapidly tracks the reference current. This is performed by a PID controller. The inverter output current in the dq0 reference frame can be calculated according to the following equations:

$$V_{d\,inv} = V_{d\,IB} + I_d R + I_q\,\omega L + L\frac{dI_d}{dt} \qquad (6)$$

$$V_{q\,inv} = I_q R - I_d\,\omega L + L\frac{dI_q}{dt} \qquad (7)$$

where $V_{d\,IB}$ is the measured voltage at PCC in the dq0 reference frame; I_d and I_q are the inverter output current in the dq0 reference frame; R is the total resistance of the filter and transformer; L is the total reactance of the filter and transformer: and ω is grid frequency in rad/s. These equations will be the planet to be controlled by a PID controller where the inputs are V_d and V_q and the outputs are $V_{d\,inv}$ and $V_{q\,inv}$, where the controlled inputs Vd and Vq.

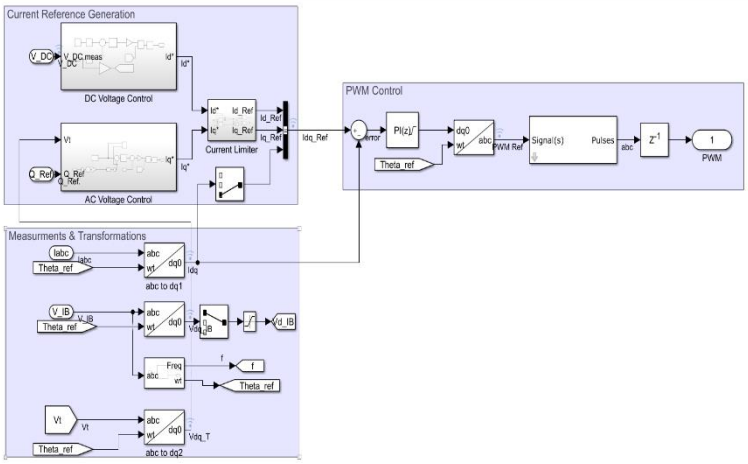

Fig.4 Inverter Control Scheme

C. Voltage Regulation of the DC Bus

The purpose of the DC regulator block is to adjust the DC-link voltage at a pre-determined value to achieve the needed output voltage level. The DC-link voltage can be determined according to the following equation,

$$C_{DC\,Link}\,\frac{dV_{DC\,Link}}{dt} = I_{Boost} - I_{inverter\,DC} \qquad (8)$$

In the DC Voltage regulator, the measured DC link voltage is compared with the reference signal, the error is sent to PID controller, and the output will be the reference direct axis current ($I_{d\,Ref}$) signal which determine the output active power as shown Fig.5

D. AC Voltage Regulation at PCC (FRT)

Fault ride through (FRT), sometimes under-voltage ride through (UVRT), or low voltage ride through (LVRT), is the capability of electric generators to stay connected in short periods of lower electric network voltage . It is needed at distribution level (wind parks, PV systems, distributed cogeneration, etc.) to prevent

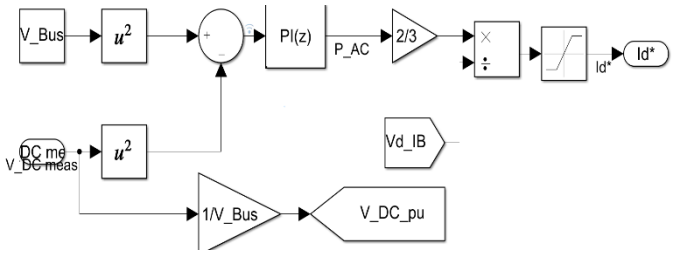

Fig.5 Control of the DC Voltage Regulation

a short circuit at HV or EHV level from causing a widespread loss of generation.

This Control is done by injecting Reactive (inductive) power during under voltages and absorb it during over voltages (as will be shown in the next section).

E. Current Limitter

This block is made to ensure that current will not exceed inverter limits. In normal operation, the priority is to inject active power to the grid, so the d-current (that controls active power) have priority over q-current, so in order to limit total current, q-component is reduced. On the other hand, in fault conditions, the priority is to inject reactive power to the grid to support it, so the q-current (that controls reactive power) have priority over d-current, so to limit total current, d-component is reduced.

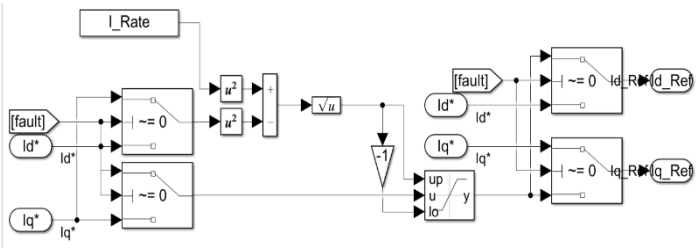

Fig.6 Inverter Current Limiter

Simulation Results and Performance Assessment:

As Shown in fig.7, the time response of both DC and AC voltages has fast response without overshooting or steady state error

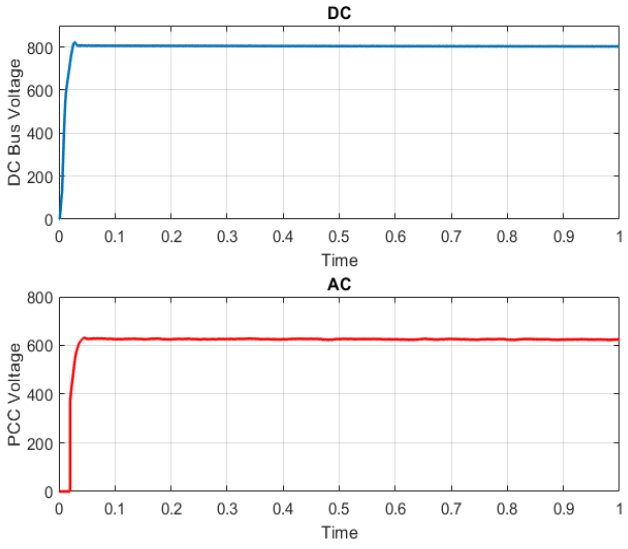

Fig.7 Inverter Voltage Regulation

Fig.8 is showing current in dq0 synchronous frame. In direct-axis, actual current is following the reference signal with small steady state error. In quadrature-axis, current is following reverence signal with approximately zero error

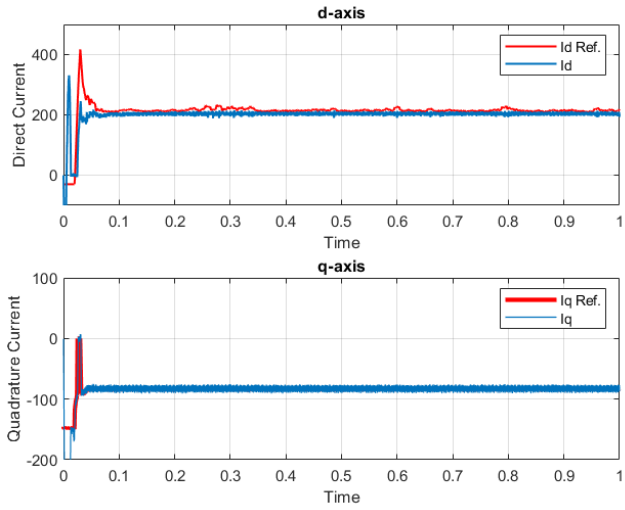

Fig.8 Inverter Current Control

In fig.9, inverter is injecting its full load power (100 kW) at 0.9 lagging p.f. (38 kVAR)

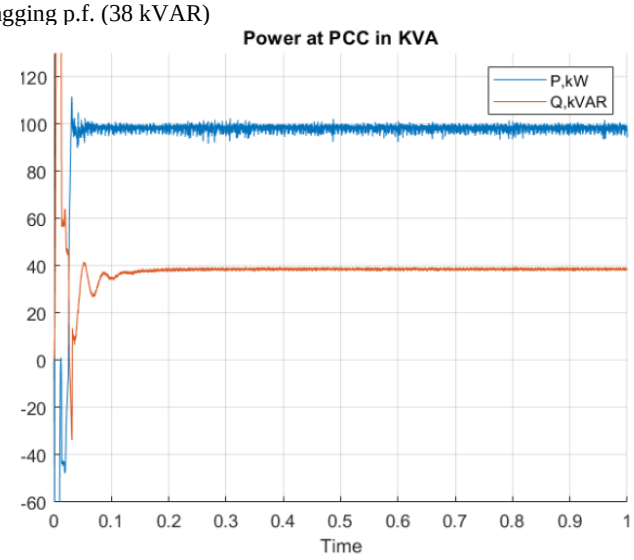

Fig.9 Injected Power at PCC

III. Tuning Gain Constants of the PID Controllers:

In this model, we used three PID controllers to control MPPT, DC Bus voltage and Power at PCC, as it's very difficult to tune four parameters for each controller (proportional Kp, integral Ki, differential Kd and filter N), we used Machine Learning Optimization algorithm called Manta ray foraging optimization (MRFO)

A. *Manta ray foraging optimization (MRFO)*

MRFO is inspired by three foraging behaviors including chain foraging, cyclone foraging and somersault foraging. The mathematical models are described below.

1) **Chain foraging**

In MRFO, manta rays can observe the position of plankton and swim towards it. The higher the concentration of plankton in a position is, the better the position is. Although the best solution is not known, MRFO assumes the best solution found so far is the plankton with high concentration manta rays want to approach and eat. Manta rays line up head-to-tail and form a foraging chain. Individuals except the first move towards not only the food but also the one in front of it. That is, in every iteration, each individual is updated by the best solution found so far and the solution in front of it.

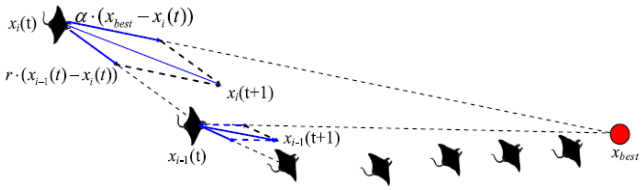

Fig.10 Chain Foraging of Manta Rays

2) ***Cyclone Foraging***

When a school of manta rays recognize a patch of plankton in deep water, they will form a long foraging chain and swim towards the food by a spiral. This similar spiral foraging strategy can be found in WOA. However, for the cyclone foraging strategy of manta ray swarms, in addition to spirally move towards the food, each manta ray swims towards the one in front of it. That is, manta ray swarms in line developing a spiral perform foraging. illustrates the cyclone foraging behavior in a 2-D space. An individual not only follows the one in front of it but only moves towards the food along a spiral path.

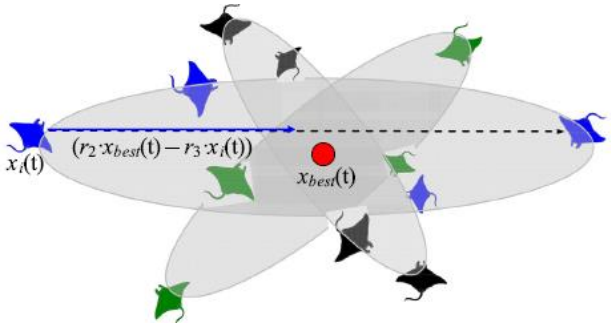

Fig.11 Cyclone Foraging of Manta Rays

3) ***Someresults Foraging***

Individuals tends to swim and fro around the pivot and somersault to a new position. Therefore, they always update their positions around the best position found so far.

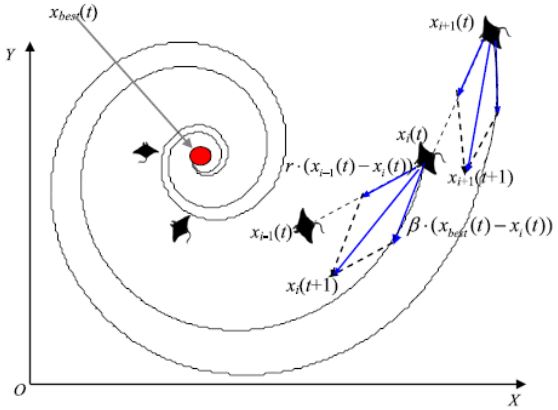

Fig.12 Someresults Foraging of Manta Rays

B. Objective

The objective is to minimize the simulation of the integral square error of all PID controllers to enhance both steady state and transient conditions

$$Obj.Fn. = \sqrt{\int_0^{t=1\ sec} \sum_{i=1}^{all\ PIDs} error_i^2(t)\ .\ dt} \quad (9)$$

C. Omtimization Results

We used MRFO algorithm with 20 population size in 100 iterations to minimize the integral square error of the PID controllers and the results were as following:

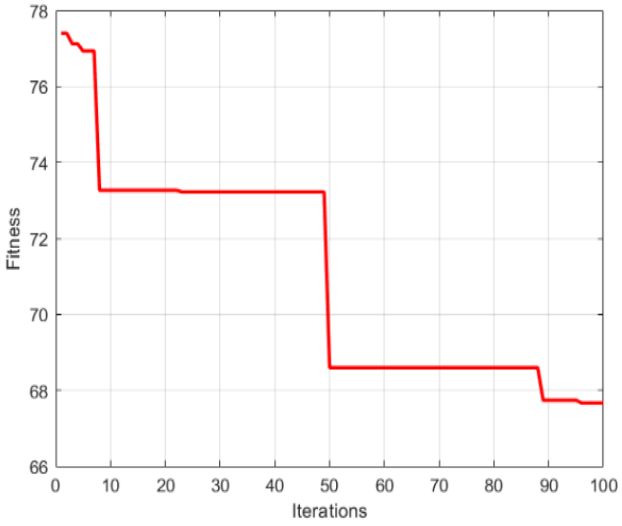

Fig.12 Objective Function Convergence of MRFO

MPPT:
Kp_MPPT = 1.1471
Ki_MPPT = 1.2366
Kd_MPPT = 0.0063
N_MPPT = 10.9859
DC Bus:
Kp_DC_Link = 2.5900
Ki_DC_Link = 19.3654
AC Bus:
Kp_AC_Q = 304.6869
Ki_AC_Q = 477.1961
Current Loop (Inverter):
Kp_Inverter = 15.2420
Ki_Inverter = 0.8247

IV. Fault Analysis

The main subject of this section is to analyze the effect of faults on the operation of the solar station, and more importantly, how this knowledge can be used to create a controller that is capable of operating during faults, furthermore, ensuring the adherence of all the solar station to the stipulated limits. The types of faults analyzed in this chapter are the one that appear in the middle of one line of the double circuit transmission line between the PCC and the grid. The faults studied will be of the single phase to ground, double phase and three phase to ground types. Simulation results will be shown and analyzed to ensure proper operation of the controller designed in dealing with the ensuing conditions.

The utility grid is composed of a double circuit transmission line (shown in the purple box Fig.1) then connected to load followed by another transmission line that is connected to the main generation station.

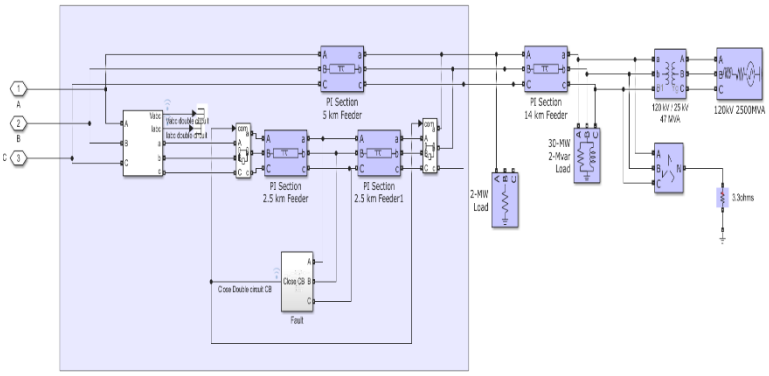

Fig.13 Utility Grid Configuration

The double circuit transmission line is two 5 Km Feeders connected in parallel, the second of which has a fault inducing Simulink block in its middle and two circuit breakers (one at the beginning of the feeder and the other at the end), the voltage and current of the second feeder are measured.

When a fault occurs, both circuit breakers trip after some delay, thus effectively leaving one feeder operational. After a prespecified time, the breakers are automatically closed. If the fault persists, the breakers trip once more.

A. Simulation Results

For every type of fault, the following graphs will be shown:

- **Fault Type:** is non-zero when there is a fault otherwise it is zero
- **Close Double Circuit Breaker:** 1 for the double circuit are both operational and 0 for the second circuit is disconnected (due to the occurrence of fault)
- **Vabc:** the three-phase voltage at the PCC in p.u.
- **Iabc IB:** the three-phase current at the PCC in p.u.
- **P Setpoint:** the active power reference that the solar station should follow
- **P measured:** the measured output active power of the solar station
- **Q Setpoint:** the reactive power reference that the solar station should follow
- **Q measured:** the measured output reactive power of the solar station
- **Capacitor Voltage:** the voltage level of the DC link capacitor in p.u.

*1) **Single phase to ground fault (LG)***

This is a fault that occurs between the red phase (phase c) and the ground.

The fault occurs at time 0.087 sec and the circuit breaker is tripped at 0.089 sec this is due to the high current that flows in the faulty line in the red phase only. The circuit breaker automatically recloses after 0.1 sec., but the fault has already disappeared 0.5 sec earlier, thus the breaker does not trip again.

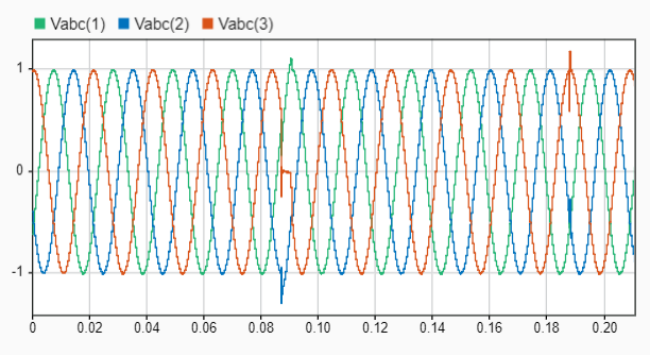

Fig.14 PCC Voltage at LG fault

The voltage seems to be pure sinusoidal except at the moment of trip and reclosing the breaker and the beginning of the fault.

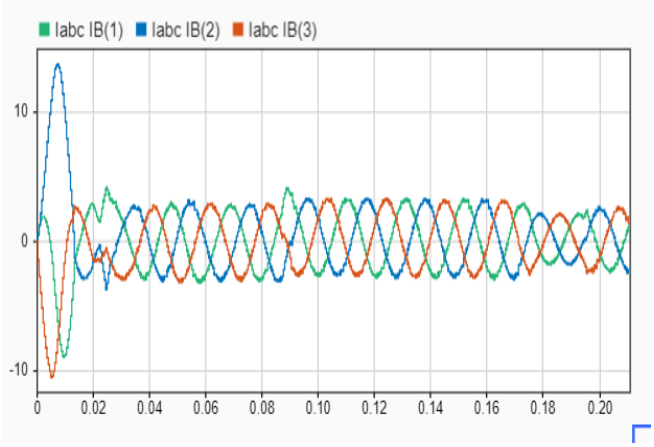

Fig.15 Injected Current at LG fault

The current at the first cycle (0.02 sec) has a transient that quickly dies, this due to the capacitor being uncharged. The current seems to be pure sinusoidal except at the moment of trip and reclosing the breaker and the beginning of the fault.

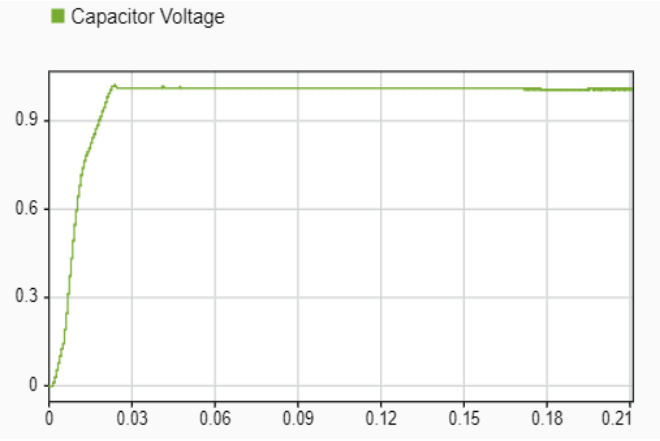

Fig.16 DC Link Capacitor Voltage at LG fault in pu

Both P and Q follow their respective varying setpoint with great accuracy despite the persistence of the fault. Thus, the controller was able to control the P and Q before, during and after the fault, except of course to the first 2 cycles where the capacitor was charging as shown in Fig.16 and Fig. 17.

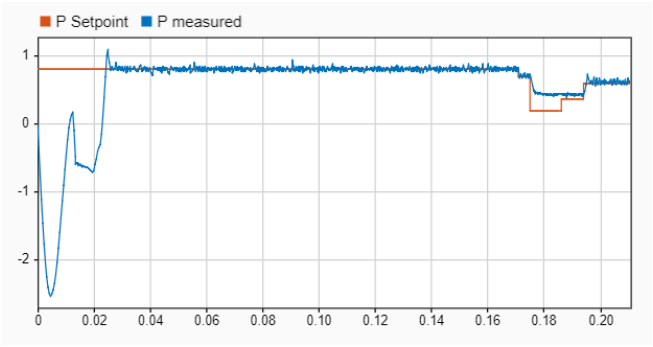

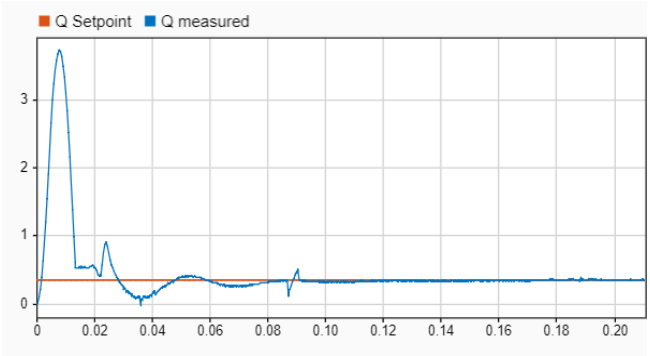

Fig.17 Active and Reactive Power at LG fault

2) ***Double phase fualt (LL)***

This is a fault that occurs between the blue and red phases (phases B & C).

The fault occurs at time 0.05 sec and the circuit breaker is tripped at 0.051 sec this is due to the high current (10 p.u.) that flows in the faulty line in the red and blue phases only as shown below. The circuit breaker automatically recloses after 0.1 sec to find that the fault did not clear, thus the breaker trip again after a delay of 0.01 sec. The fault is cleared at 0.17 sec.

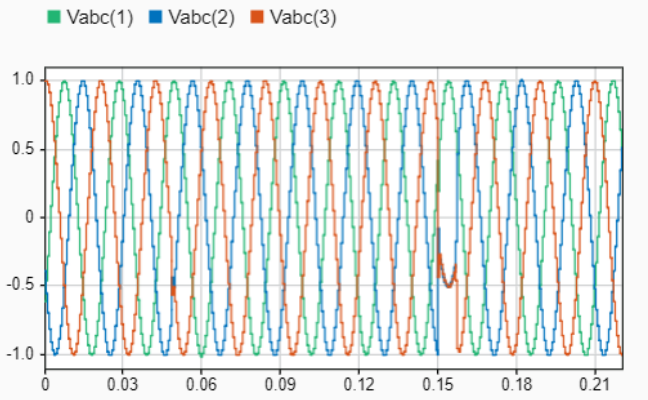

Fig.18 PCC Voltage at LL fault

The voltage seems to be pure sinusoidal except at the moment of trip and reclosing the breaker and the beginning of the fault. The green phase seems to be unaffected by the fault as expected.

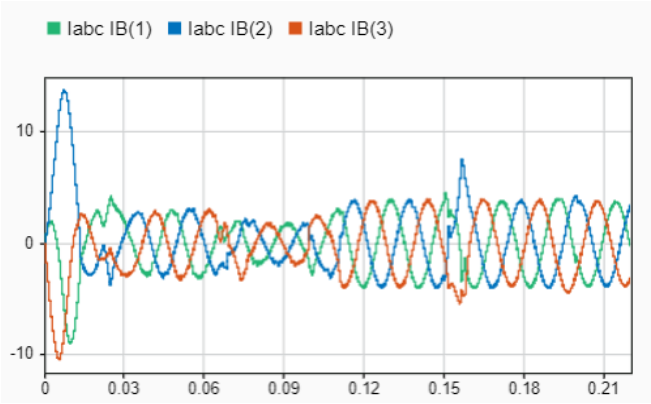

Fig.19 Injected Current at LL fault

The current at the first cycle (0.02 sec) has a transient that quickly dies, this due to the capacitor being uncharged. The current seems to be pure sinusoidal except at the moment of trip and reclosing the breaker and the beginning of the fault.

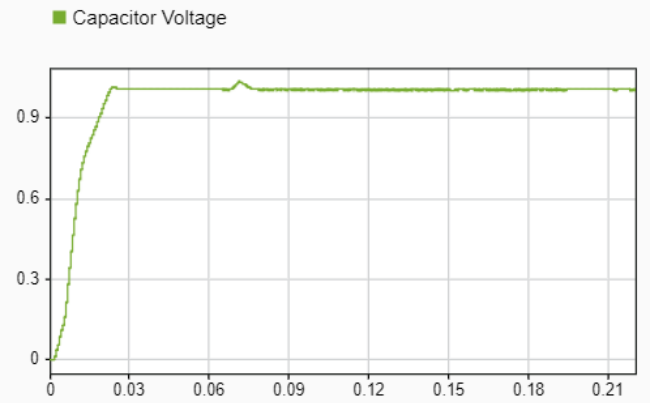

Fig.20 DC Link Capacitor Voltage at LL fault in pu

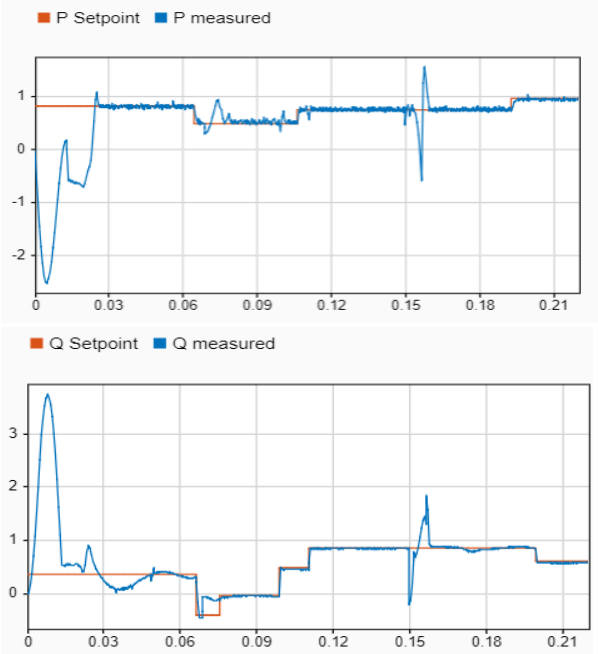

Fig.21 Active and Reactive Power at LL fault

Both P and Q follow their respective varying setpoint with great accuracy despite the persistence of the fault. Thus, the controller was able to control the P and Q before, during and after the fault, except of course to the first 2 cycles where the capacitor was charging as shown in Fig.20 and Fig. 21.

*3) **Three-phase to ground fault (LLLG)***

This is a fault that occurs between the three phases and the ground.

The fault occurs at time 0.06 sec and the circuit breaker is tripped at 0.061 sec this is due to the high current (500 p.u.) that flows in the faulty line as shown below. The circuit breaker automatically recloses after 0.1 sec to find that the fault did not clear, thus the breaker trip again after a delay of 0.01 sec. The fault is cleared at 0.19 sec.

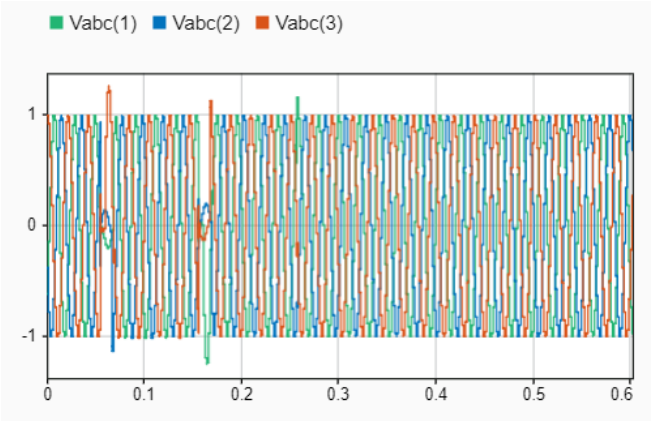

Fig.22 PCC Voltage at LLLG fault

The voltage seems to be pure sinusoidal except at the moment of trip and reclosing the breaker and the beginning of the fault.

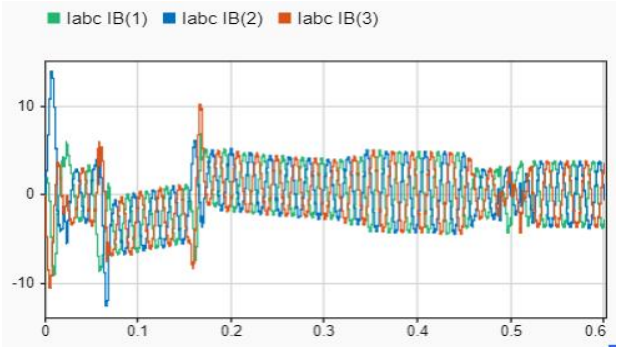

Fig.23 Injected Current at LLLG fault

The current at the first cycle (0.02 sec) has a transient that quickly dies, this due to the capacitor being uncharged. The current seems to be pure sinusoidal except at the moment of trip and reclosing the breaker and the beginning of the fault. The current seems to have a DC transient component that dies of this DC component appears after the switching instants of the second circuit of the double transmission line. At steady state, this component decays completely.

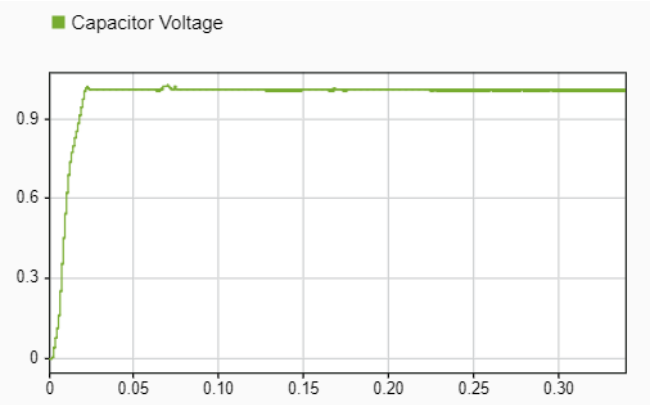

Fig.24 DC Link Capacitor Voltage at LLLG fault in pu

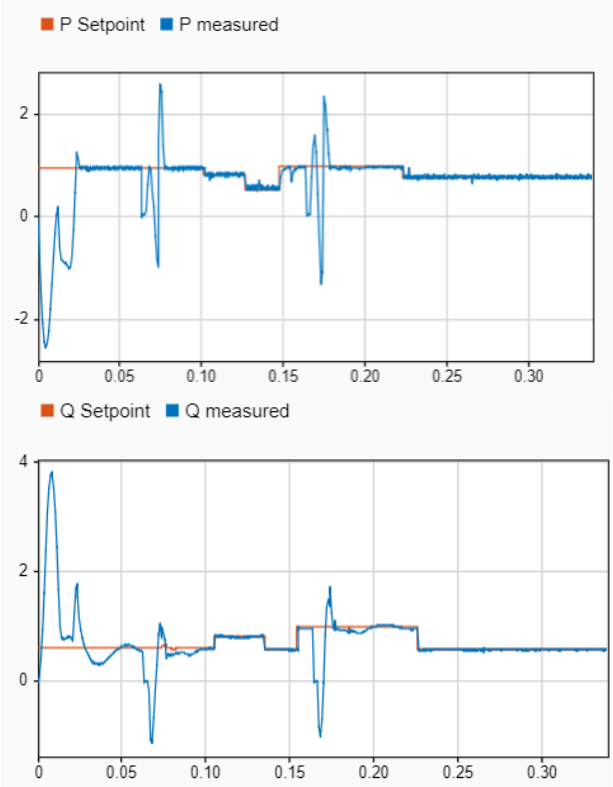

Fig.25 Active and Reactive Power at LLLG fault

Both P and Q follow their respective varying setpoint with great accuracy despite the persistence of the

fault. Thus, the controller was able to control the P and Q before, during and after the fault, except of course to the first 2 cycles where the capacitor was charging as shown in Fig.24 and Fig. 25.

REFERENCES

[1] Modeling and Control of Sustainable Power Systems: Towards Smarter and Greener Electric Grids. Prof. LingfengcWang University of Toledo

[2] Dynamics and stability of conventional and renewable energy systems: Mohamed EL-Shimy Ain Shams University

[3] Manta ray foraging optimization: An effective bio-inspired optimizer for engineering applications: Weiguo Zhao, Zhenxing Zhang, Liying Wang

[4] Optimization of Photovoltaic Power Using PID MPPT Controller Based on Incremental Conductance Algorithm: B. Ashok Kumar, M. Srinivasa Venkatesh and G. Mohan Muralikrishna

[5] Cascaded Control Scheme of Grid Tied PV inverter: Muhammed H. Abbasi, hany M. Hassanien, Abdulhameed Al_Ohaly, Yasin Khan

[6] Fault Ride-Through Enhancement of Grid Supporting Inverter-Based Microgrid Using Delayed Signal Cancellation Algorithm Secondary Control Elutunji Buraimoh , Innocent E. Davidson and Fernando Martinez-Rodrigo

[7] Fault ride through capability for grid interfacing large scale PV power plants. Mohamed Shawky El Moursi1,2, Weidong Xiao2, Jim. L. Kirtley Jr1

[8] An Adaptive Control Strategy for Low Voltage Ride Through Capability Enhancement of Grid-Connected Photovoltaic Power Plants – Hany M. Hasanien, Senior Member, IEEE (2016)

[9] Mulukutla S. Sarma - Power System Analysis and Design (2017)

[10] Yoshihide Hase - Power System Dynamics with Computer-Based Modeling and Analysis (2020)

[11] A. Abdalrahman, A. Zekry, And A. Alshazly, (2012), "Simulation and Implementation of Grid-Connected Inverters", International Journal of Computer Applications, Vol.60, No.4, pp. 41–49.

[12] N. Altin, and S. Ozdemir, (2013), "Three-Phase Three-Level Grid Interactive Inverter with Fuzzy Logic Based Maximum Power Point Tracking Controller", Journal of Energy Conversion and Management. Vol. 69 (2013), pp. 17-26.

[13] Parameters extraction of PEMFC's model using manta rays foraging optimizer, Sameh I. Selem, Hany M. Hasanien and Attia A. El-Fergany

[14] Optimal design of automatic voltage regulation controller using hybrid simulated annealing – Manta ray foraging optimization algorithm Mihailo Micev, Martin C´ alasan, Ziad M. Ali, Hany M. Hasanien, Shady H.E. Abdel Aleem

[15] Cespedes, M. and Sun, J. (2014), "Adaptive Control of Grid-Connected Inverters Based On Online Grid Impedance Measurements", IEEE Trans-actions on Sustainable Energy. IEEE, Vol. 5, No. 2, pp.516–523.

[16] P.Chan, and S. Masri, (2010), "DC-DC Boost Converter with Constant Output Voltage for Grid Connected Photovoltaic Application System", 2010 International Conference on Intelligent and Advanced Systems, Manila, Philippines, pp. 1-4.

[17] D. Das, and S. K. P. Pradhan, (2011), "Modeling and Simulation of PV Array With Boost Converter : An Open Loop Study", Unpublished B. Tech. Project Report, National Institute of Technology, Rourkela, 47 pp.

[18] Faisal, S.M. A. (2012), "Model of Grid-Connected Photovoltaic System Using MATLAB / SIMULINK", International Journal of Electrical Engineering, Vol. 12, pp. 173 -184.

[19] Hannan, M. A., Zambre, A. G., Mohammed, A., and Uddin, M. N. (2015), "Real-Time Testing of A Fuzzy Logic Controller Based Grid Connected Photovoltaic Inverter System", IEEE Transactions on Industry Applications, Vol. 51, No. 1, pp. 4775 – 4784.

[20] Y. Jia, J. Zhao, and X. Fu. (2014), "Direct Grid Current Control of LCL-Filtered Grid-Connected Inverter Mitigating Grid", IEEE Transactions on Power Electronics, Vol. 29, No. 3, pp. 1532–1541.

[21] M. N. Ambia, H. M. Hasanien, A. Al-Durra, and S. M. Muyeen, "Harmony search algorithm-based controller parameters optimization for a distributed-generation system," IEEE Trans. Power Del., vol. 30, no. 1, pp. 246–255, Feb. 2015.

[22] H. M. Hasanien, "Shuffled frog leaping algorithm-based static synchronous compensator for transient stability improvement of a gridconnected wind farm," IET Renew. Power Gener., vol. 8, no. 6, pp. 722–730, Aug. 2014.

[23] J. Ni and F. Li, "Efficient implementation of the affine projection sign algorithm," IEEE Signal Process. Lett., vol. 19, no. 1, pp. 24–26, Jan. 2012